Atomic-scale finite element modelling of mechanical behaviour of graphene nanoribbons

D.A. Damasceno[1], E. Mesquita[1], R.K.N.D. Rajapakse[2] and R. Pavanello[1]

[1]Department of Computational Mechanics, University of Campinas, Campinas, Brazil

[2]School of Engineering Science, Simon Fraser University, Burnaby, Canada V5 1S6

Abstract: Experimental characterization of Graphene NanoRibbons (GNRs) is still an expensive task and computational simulations are therefore seen a practical option to study the properties and mechanical response of GNRs. Design of GNR in various nanotechnology devices can be approached through molecular dynamics simulations. This study demonstrates that the Atomic–scale Finite Element Method (AFEM) based on the second generation REBO potential is an efficient and accurate alternative to the molecular dynamics simulation of GNRs. Special atomic finite elements are proposed to model graphene edges. Extensive comparisons are presented with MD solutions to establish the accuracy of AFEM. It is also shown that the Tersoff potential is not accurate for GNR modeling. The study demonstrates the influence of chirality and size on design parameters such as tensile strength and stiffness. A GNR is stronger and stiffer in the zigzag direction compared to the armchair direction. Armchair GNRs shows a minor dependence of tensile strength and elastic modulus on size whereas in the case of zigzag GNRs both modulus and strength show a significant size dependency. The size-dependency trend noted in the present study is different from the previously reported MD solutions for GNRs but qualitatively agrees with experimental results. Based on the present study, AFEM can be considered a highly efficient computational tool for analysis and design of GNRs.

Keywords: Atomistic simulation, elastic modulus, graphene, nanoribbons, tensile strength

1. Introduction

The separation of carbon allotrope "graphene" (a single flat atomic layer of graphite) using mechanical exfoliation (Novoselov et al. 2004) and advances in nanofabrication have opened the door for the bottom-up approach to nanotechnology. In this approach, nanodevices are built from basic atomic structures such as Graphene NanoRibbons (GNRs), Carbon NanoTubes (CNT), etc. Graphene and other nanomaterials allow for the design and fabrication of a new generation of composites and nanoelectromechanical systems with attractive mechanical, electronic and optical properties (Choi and Lee 2016; Chen and Hone 2013).

The mechanical behaviour of nanoscale systems can be analyzed by using ab-initio (first-principle) methods (Hohenberg and Kohn 1964) or semi-empirical quantum methods (Haile 1992). Ab-initio calculations are computationally very expensive, and modelling is limited to a few hundred or thousand atoms. Semi-empirical quantum methods such as Molecular Dynamics (MD) and Tight-Binding Method (TBM) are used to simplify atomistic simulations. The parameters in MD and TBM are empirical, fitted to experimental data. MD has been one of the most commonly used methods to analyze the behaviour of nanomaterials. It solves the dynamic equilibrium state of an atomic system to obtain time-dependent positions of atoms under excitation. Even MD is computationally expensive when applied to systems with a very large number of atoms.

An alternate approach to MD analysis is the Atomic Scale Finite Element Method (AFEM) proposed by Liu et al. (2004). Unlike MD, it is a quasi-static solution of the final equilibrium state of an atomic system and requires no time integration. It serves as a computationally efficient alternative to MD because of its O(N) computational characteristics. Note that other available atomic simulation methods are at least $O(N^2)$. The formulation of AFEM resembles the classical finite element method (FEM) and uses the total energy of an atomic system based on its potential field to derive the stiffness matrix and force vector. The stiffness is dependent on the positions of atoms, hence, non-linear. The method requires an iterative solution to obtain equilibrium state. It is considered superior to the beam/spring models for C-C bonds proposed by Tserpes and Papanikos (2005) and Alzebdeh (2012) as complex potential fields that take into account many body interactions can be used to simulate the behaviour of atomic systems. A number of studies have confirmed the accuracy of AFEM in modelling CNT and carbon nanorings and their global behaviour such as buckling loads and free vibration characteristics (Liu et al. 2004, 2005; Shi et al. 2009; Ghajbhiye and Singh 2015). However, comprehensive comparisons of AFEM with MD simulations are limited in the literature.

In recent years, the use of single-layer (SL) and multi-layer (ML) GNRs have been demonstrated through experiments for applications ranging from resonators and sensors to reinforcing elements in

polymer composites (Choi and Lee 2016; Chen and Hone 2013; Njugna and Pielichowski 2003). Unlike CNT, GNRs are 2-D structures that have a wide range of applications. As nanofabrication is still an expensive and challenging task and material characterization at the nanoscale is not yet a mature technology, there is considerable interest in atomistic modelling to assess properties, design nanodevices and understand their performance and reliability. Simulations can be used to determine the final design parameters for fabrication. In this regard, AFEM could serve as an efficient modelling tool for preliminary design of nanomaterials and nanodevices that can be verified at the final design and fabrication stage using more comprehensive atomistic simulations such as MD. Although the application of AFEM to CNT modelling has been demonstrated (Liu et al. 2004, 2005; Shi et al. 2009), its application to the modelling of GNR has attracted no attention according to our knowledge.

Several fundamental design-related issues require attention in the case of GNRs. While most atomistic simulation studies on graphene have focused on bulk graphene where Periodic Boundary Conditions (PBC) are used, GNRs have edges that could have a significant effect on design parameters such as tensile strength and elastic modulus (Fig. 1). The common GNR edges are either armchair or zigzag or they could be described by using an arbitrary chiral vector expressed in terms of the hexagonal base vectors n_1 and n_2 shown in Fig. 1. CNTs are considered 1-D structures and end (edge) effects are not significant in most applications. Several recent studies (Chu et al. 2014; Le 2015; Ng et al. 2013; Zhao et al. 2009) have used molecular dynamics and molecular mechanics to examine the mechanical and thermal properties of GNRs. Furthermore, as shown by Zhao et al. (2009) and Chu et al (2014) using MD simulations, the above design parameters are strongly size and chirality dependent. It would therefore be useful to establish the applicability of AFEM as a design tool for GNRs through a comprehensive comparison with MD results and examine the size and chirality dependence of tensile strength and elastic modulus based on AFEM.

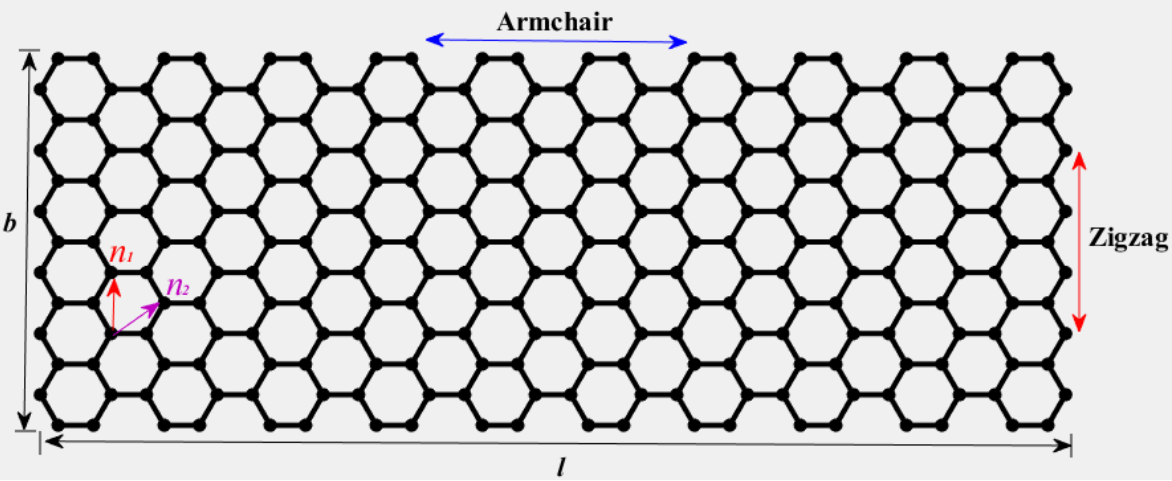

Figure 1: Armchair and zigzag edges of graphene nanoribbon.

Recent studies by Malakouti and Montazeri (2016) and Gajbhiye and Singh (2015) demonstrated the application of AFEM to analyze pristine and defective bulk graphene sheets and nonlinear frequency response respectively. While both these studies have not examined size-dependency, and edge and chirality effects of GNRs, they are also based on the Tersoff-Brenner (T-B) potential (Brenner 1990; Tersoff 1988). The T-B potential has certain deficiencies as reported by Brenner et al. (2002) and Stuart et al. (2000). It does not have a double bond or conjugate bond rotation barrier to prevent certain unrealistic bond rotations. The second generation Reactive Empirical Bond Order (REBO) potential proposed by Brenner et al. (2002) leads to a significantly better description of bond energies, lengths, and force constants for hydrocarbon molecules, as well as elastic properties thus enabling simulation of complex deformation patterns. It also accounts for forces associated with rotation about dihedral angles for carbon–carbon double bonds.

Based on the above literature review, this paper has several objectives. We first implement the Tersoff potential (Tersoff 1988) and second generation REBO potential (Brenner et al. 2002) in AFEM to assess the dependence of potential field in AFEM modelling of GNRs and compare with MD simulation results for bulk graphene. We thereafter compare the tensile strength and elastic modulus of GNRs and bulk graphene obtained from AFEM using the two potentials with MD simulations for different chiralities. Through these comparisons, we demonstrate the deficiencies of Tersoff potential in modelling GNRs and establish that AFEM based on the second generation REBO is a very efficient and accurate approach to simulate the mechanical response of GNRs. Next, we focus on the size-dependency of tensile strength and elastic modulus of GNRs of different width to length ratios. Through these studies, we demonstrate that AFEM can be used as an accurate and efficient simulation tool for design of GNRs.

2. Atomic-scale Finite Element Method (AFEM)

2.1 Formulation

In the AFEM formulation proposed by Liu et al. (2004), the equilibrium configuration of the atomic system in relation to the position of the atoms, $\boldsymbol{x}$, is related to the state of minimal energy as,

$$\frac{dE_{tot}}{d\boldsymbol{x}} = 0 \tag{1}$$

The total energy E_{tot} can be expanded in a Taylor series around the equilibrium position $\boldsymbol{x}^{(0)}$:

$$E_{tot}\left(\boldsymbol{x}\right) \approx E_{tot}\left(\boldsymbol{x}^{(0)}\right) + \left.\frac{dE_{tot}}{d\boldsymbol{x}}\right|_{\boldsymbol{x}=\boldsymbol{x}^{(0)}} \left(\boldsymbol{x}-\boldsymbol{x}^{(0)}\right) + \frac{1}{2}\left(\boldsymbol{x}-\boldsymbol{x}^{(0)}\right)^{T} \left.\frac{d^{2}E_{tot}}{d\boldsymbol{x}d\boldsymbol{x}}\right|_{\boldsymbol{x}=\boldsymbol{x}^{(0)}} \left(\boldsymbol{x}-\boldsymbol{x}^{(0)}\right) \tag{2}$$

Defining the displacement $\boldsymbol{u}$ as:

$$\boldsymbol{u} = \left(\boldsymbol{x} - \boldsymbol{x}^{(0)} \right) \tag{3}$$

Then substitute the Eq. (2) into Eq. (1) to give the following AFEM equation system, which is similar to the governing equation in FEM:

$$\boldsymbol{K\Delta u} = \boldsymbol{P} \tag{4}$$

where $\boldsymbol{K}$ corresponds to the nonlinear stiffness matrix; $\boldsymbol{\Delta u}$ is the displacement increment vector; and $\boldsymbol{P}$ is the non-equilibrium load vector respectively given by:

$$\boldsymbol{K} = \left. \frac{d^2 E_{tot}}{d\boldsymbol{x} d\boldsymbol{x}} \right|_{\boldsymbol{x} = \boldsymbol{x}^{(0)}} \tag{5}$$

$$\boldsymbol{P} = - \left. \frac{dE_{tot}}{dx} \right|_{x = x^{(0)}} \tag{6}$$

The total energy consists of the sum of internal energy stored within each atomic bond, U, and the work done by the external forces, W_f. For a system with N atoms the interatomic total energy, U_{tot}, is given by:

$$U_{tot} = \sum_{i<j}^{N} U\left(\boldsymbol{x}_j - \boldsymbol{x}_i \right) \tag{7}$$

In Eq. (7), U corresponds to a pairwise potential. The work done by the external forces, F_i^{ext}, acting on the i^{th} atom is given by:

$$W_f = \sum_{i=1}^{N} F_i^{ext} \boldsymbol{x}_i \tag{8}$$

Considering Eqs. (7) and (8) the total energy of the system is given by:

$$E_{tot} = \sum_{i<j}^{N} U\left(\boldsymbol{x}_j - \boldsymbol{x}_i\right) - \sum_{i=1}^{N} F_i^{ext}\boldsymbol{x}_i \tag{9}$$

The computational procedure of AFEM involves four steps. The first step is the construction of the element stiffness matrix, ***K***, and element non-equilibrium force vector, ***P***. Next, build the global stiffness matrix and global non-equilibrium force vector, and then solve Eq. (4). Finally, update the displacement vector. As the basic formulation of AFEM described by Eq. (4) is nonlinear, it must be solved iteratively until the global non-equilibrium force vector, ***P***, reaches zero within a prescribed tolerance.

2.2 Tersoff Potential

Similar to MD, the accuracy of AFEM for a given atomic system depends on the potential field chosen to describe the atomic interactions. One of the earliest many-body potential is the Tersoff potential (Tersoff 1987; Tersoff 1988) which contains a bond-order term. The energy stored in the bond between atoms *i* and *j* is given as a function of the separation distance (r_{ij}) between the atoms and expressed as,

$$V^T = f_c^T\left(r_{ij}\right)\left[V_R^T\left(r_{ij}\right) + B^T V_A^T\left(r_{ij}\right)\right] \tag{10}$$

where $f_c^T\left(r_{ij}\right)$ is a cut-off function that is defined in Appendix; V_R^T and V_A^T represent the repulsive and attractive pair potential in relation to r_{ij} respectively; and B^T is a monotonically decreasing function and expresses the measure of the bond order, which is related to the number of neighbors and bond angles.

$$V_R^T\left(r_{ij}\right) = Aexp\left(-\lambda^1 r_{ij}\right);\ V_A^T\left(r_{ij}\right) = -Bexp\left(-\lambda^2 r_{ij}\right)\ ;\ B^T = \left(1+\beta^{n_T}\zeta_{ij}^{n_T}\right)^{-\left(\frac{1}{2n_t}\right)} \tag{11}$$

Additional parameters appearing in Eqs. (10) and (11) are defined in Appendix.

2.3 Second Generation REBO Potential

The second-generation REBO potential (Brenner et al., 2002) is an advanced improvement of the Tersoff potential. The energy stored on the bond between atoms *i* and *j* is given by:

$$V^R = f_c^R\left(r_{ij}\right)\left(V_R^R + B^R V_A^R\right) \tag{12}$$

where,

$$V_R^R = \left[1 + \frac{Q_{ij}}{r_{ij}}\right] A_{ij} e^{-\alpha_{ij} r_{ij}} \; ; \; V_A^R = -\sum_{n=1}^{3} B_{ij}^{(n)} e^{-\beta_{ij}^{(n)} r_{ij}} \tag{13}$$

and the parameters Q_{ij} , A_{ij} , α_{ij} , $B_{ij}^{(n)}$ and $\beta_{ij}^{(n)}$ depend on the atom types *i* and *j*; r_{ij} is the bond length.

The term B^R corresponds to the bond order term. It is related to the number of neighbors and the angle, which is related to the forming and breaking of the bonds between the atoms. It is defined as,

$$B^R = \frac{1}{2}\left[b_{ij}^{\sigma\pi} + b_{ji}^{\sigma\pi}\right] + b_{ij}^{\pi} \tag{14}$$

Additional parameters involved in Eqs. (12) - (14) are defined in Appendix

3. Atomic Finite Elements

Figure 2 shows the basic atomic finite element for Tersoff and second generation REBO potentials for graphene. The central atom (1) interacts with three nearest neighbouring atoms 2, 5 and 8 and the six second nearest neighbouring atoms 3, 4, 6, 7, 9 and 10. The complete element is applicable at the interior of bulk graphene where the stiffness of interior atoms are computed using a complete atomic finite element. However for GNRs, the edge effects could be significant depending on the dimensions of the nanoribbon. It is therefore necessary to consider the exact connectivity of edge atoms and derive the stiffness matrix for all possible atomic finite element configurations of edge atoms. Figure 3 shows the possible edge atom connectivity for GNR edges. There are six possible atomic element configurations for edge atoms for both armchair and zigzag configurations. Each of these modified atomic finite elements has less than nine neighbouring atoms compared to Fig. 2. It should be noted that the stiffness of these modified atomic finite elements cannot be obtained by simply dropping the relevant rows and columns of the element shown in Fig. 2. The energy of each edge atom should be derived based on the exact connectivity using the relevant potential (Tersoff or second generation REBO) and the corresponding stiffness matrix derived for each case.

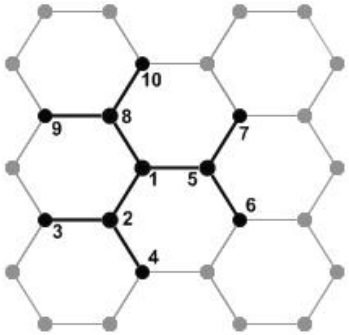

Figure 2 Graphene sheet and the basic atomic finite element.

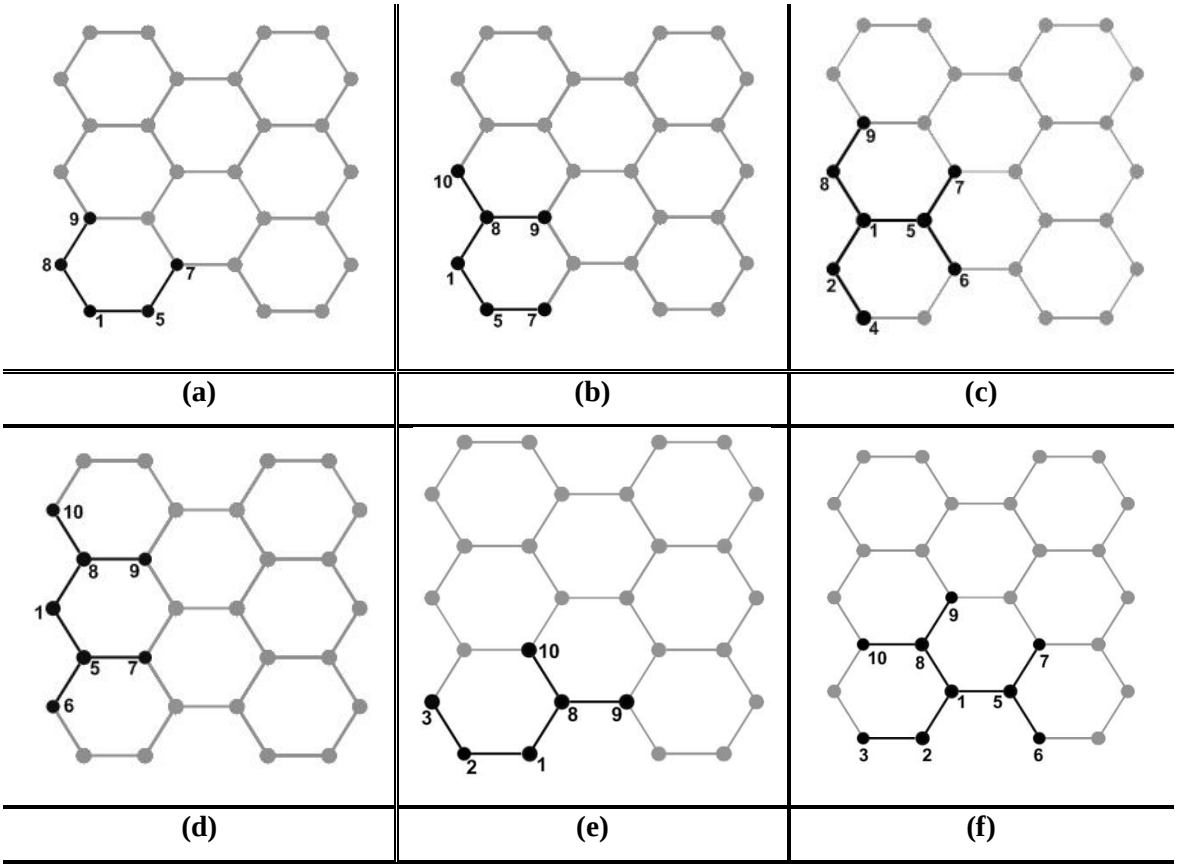

Figure 3: Modified atomic finite elements for edge atoms.

4. Numerical Results and Discussion

In this section, the mechanical behaviour of single layer graphene sheets obtained from AFEM simulations is presented and material characteristics relevant to the design of GNRs are examined.

4.1 Verification of the accuracy of AFEM

Initially, in order to validate the AFEM implementation, the stress-strain curves of pristine bulk graphene sheets under tension are compared with molecular dynamics (MD) simulation results. The

Tersoff and second generation REBO potential simulations were carried out at a temperature of 1 K. Non-periodic boundary conditions were used in MD and AFEM modeling involved edge elements as described above. The canonical ensemble (NVT) together with a time integration step of 0.5 fs was used in MD. The equilibrium distance between two carbon atoms was taken as 1.396 Å (Stuart et al. 2000). The Tersoff and second generation REBO potential parameters used in this study can be found in Tersoff (1988) and Stuart et al. (2000) respectively. Two pristine graphene sheet having armchair and zigzag edges with dimensions of 23.7 Å x 21.8 Å (228 atoms) and 41.2 Å x 39.4 Å (660 atoms) were subjected to uniaxial tension loading to examine the accuracy and size effects of AFEM. The atomic mesh corresponding to the 660 atoms case is shown in Fig. 4 with tensile loading configurations for the armchair and zigzag directions. In computing stresses, the thickness of sheet was assumed as 0.34 nm. Modified Newton-Raphson method was used to solve the Eq. (4) with load steps of 0.1 eV/ Å.

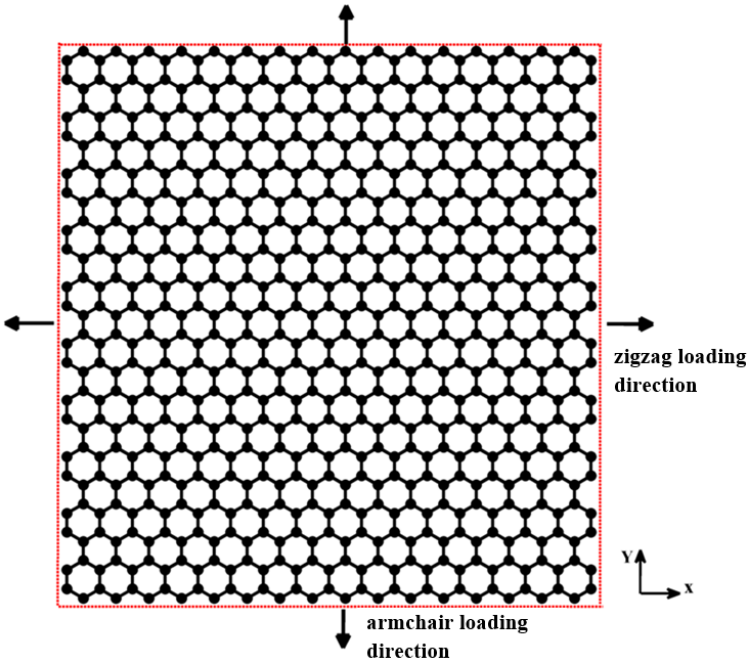

Figure 4. Graphene sheet with 660 atoms and tensile loading in armchair and zigzag directions.

Figure 5a shows a comparison of the stress-strain curves of pristine graphene sheets obtained from AFEM and MD simulations for uniaxial tensile loading in the armchair and zigzag directions based on the Tersoff potential. Note that engineering (nominal) stress and strain are used in the calculations. The results for 228 and 660 atoms meshes showed minor differences confirming that the considered mesh sizes were sufficient to model the behaviour of bulk graphene. Therefore, the solutions are only shown for the 660 atoms mesh. The AFEM and MD results agree very closely until strain reaches 0.1 and thereafter show minor deviation with MD results showing slightly higher softening. Minor oscillations are quite natural in MD simulations as the response is determined through a dynamic

analysis and nominal stress does not contain a correction for the kinetic energy of the system (Dewapriya 2012). AFEM results are quite smooth as they correspond to quasi-static analysis. Some deviations are observed at higher strains closer to the ultimate strength as MD better simulates the initial bond breaking until the solution becomes unstable and reaches the failure point (Dewapriya and Rajapakse 2014). It is therefore observed that failure strains from MD simulations are slightly higher and ultimate strengths are slightly smaller. AFEM in the current form does not capture bond breaking as well as MD but the behaviour shown in Fig. 5a confirms that it is able to capture the failure stress and strain predicted by MD with good accuracy.

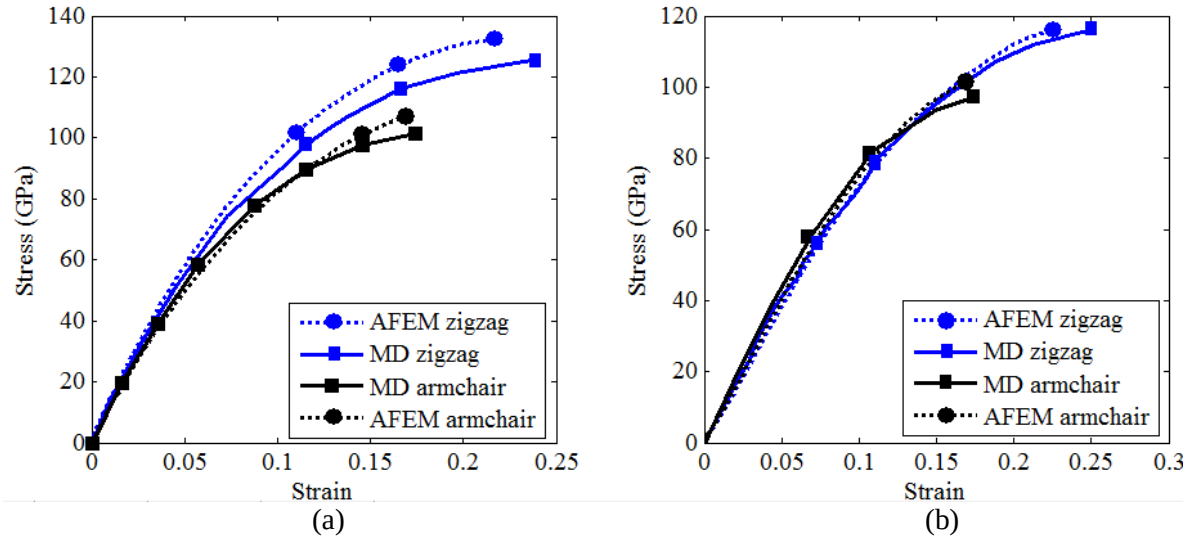

Figure 5 Stress-strain curves obtained from AFEM and MD for armchair and zigzag sheets based on (a) Tersoff potential and (b) the second generation REBO potential.

Although the results in Fig. 5a for AFEM and MD simulations are generally in good agreement, it is known that the Tersoff potential has certain weaknessess in modelling carbon atom systems (Stuart et al. 2000). Figure 5b shows the stress-strain curves based on the second generation REBO potential. Here again, very good agreement between the AFEM and the corresponding MD results is noted. In fact, the agreement between MD and AFEM is better. However, there are clear differences in the stress-strain curves presented in Fig. 5a and 5b for the different chiralities and potentials. These differences are illustrated in Fig. 6 where the AFEM-based stress-strain curves obtained from the two different potential functions are compared with an independent MD simulation reported in the literature (Zhao et al. 2009).

Figure 6 shows that the stress-strain curves based on the Tersoff potential have a strong chirality dependence whereas the results from the second generation REBO potential are nearly independent of the chirality except for the different tensile strengths and failure strains. The second generation REBO results in Fig. 6 agree quite closely with the results of Zhao et al. (2009), who used the orthogonal tight-

binding method and molecular dynamic simulations based on the AIREBO potential (Stuart et al. 2000) to obtain their stress-strain curves. AIREBO is a more advanced version of the REBO potential and the second generation REBO results obtained from AFEM is as good as the AIREBO solutions although the AFEM computational cost is only a fraction of the MD computation cost. The deficiencies of the Tersoff potential in modelling the behaviour of graphene is clear from the Fig. 6 and it is therefore not used in GNR modelling in the remainder of this paper.

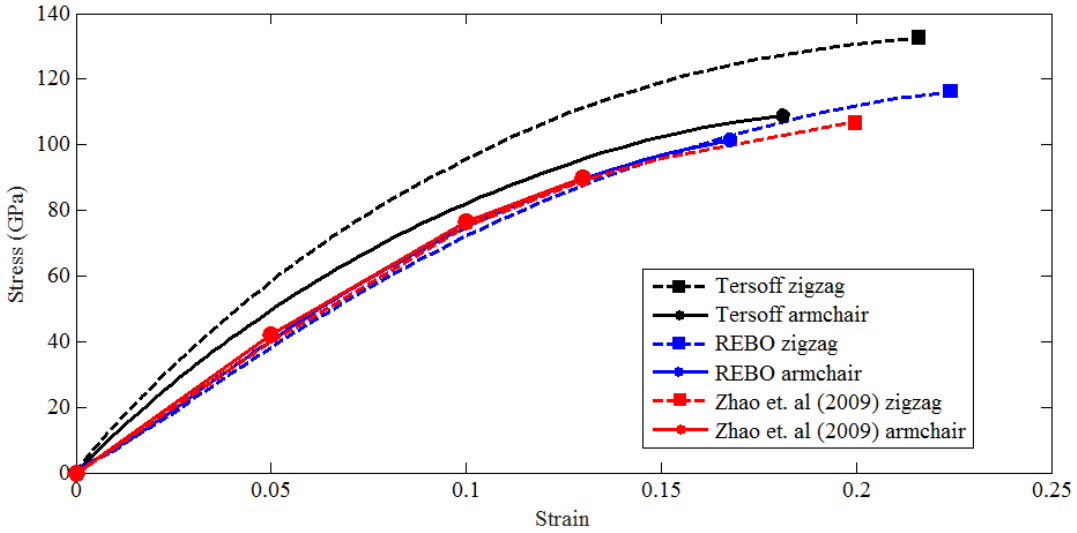

Figure 6 Comparison of stress-strain curves of pristine bulk graphene obtained from AFEM using Tersoff and second generation REBO potentials with AIREBO potential based MD results.

The ultimate tensile strength obtained from AFEM is 101.3 GPa and 116.4 GPa in the armchair and zigzag cases respectively. The fracture strain also depends on the chirality, and is 0.17 and 0.23 in the armchair and zigzag directions respectively. The elastic modulus is 0.67 TPa for armchair and 0.71 TPs for zigzag. Zhao et al. (2009) used MD simulation and reported fracture strain and tensile as 0.13 and 90 GPa in the armchair direction, and 0.2 and 107 GPa in the zigzag direction. Lee et al. (2008) reported, based on experimental measurements, an elastic modulus and intrinsic breaking strength of 1±0.1 TPa and 130 ± 10 GPa respectively for bulk graphene. Liu et al. (2007) using ab initio calculations reported an elastic modulus of 1.050 TPa and tensile strengths of 110 and 121 GPa in the armchair and zigzag directions respectively. Based on ab initio calculations, an elastic modulus of 1.11 TPa (Liera et al. 2000) and 1.24 ± 0.01 TPa (Konstantinova et al. 2006) has been reported in the literature. Using atomistic simulations, Terdalkar et al. (2010) reported an elastic modulus of 0.84 TPa. Cao (2014) presented a comprehensive review of MD simulations of graphene and highlighted the differences between properties reported by different methods. The results obtained from the AFEM based on the second generation REBO potential agree quite well with the above reported solutions tensile strength but lower for the elastic modulus. It should be noted that results from various studies (both experimental and simulations) reported in the literature do not agree perfectly with each other due to different

simulation conditions and assumptions (Cao 2014). Generally, the tensile strength reported is in the range 90-130 GPa and elastic modulus around 0.7-1.1 TPa.

Further comparisons of stress-strain curves of bulk graphene obtained from AFEM based on the second generation REBO potential is shown in Fig. 7 where the MD simulation results of Dewapriya (2012) and Malakouti and Montazeri (2016) are used. The present results agree closely with Dewapriya (2012) who used the AIREBO potential but deviate from Malakouti and Montazeri (2016) at higher strains whose results appeared to be based on the first generation REBO potential. Based on these comparisons, it is clear that AFEM based on the second generation potential is able to accurately simulate the tensile response of bulk graphene.

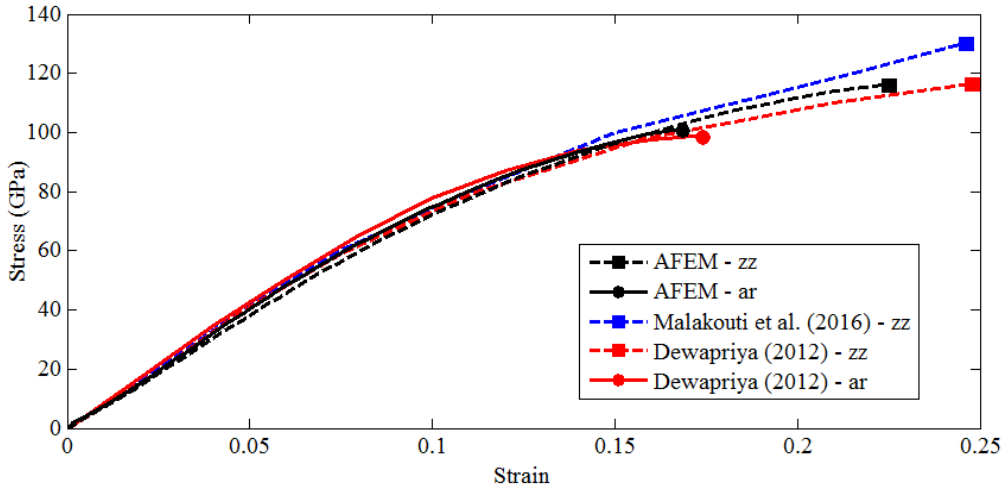

Figure 7. Comparison of stress-strain curves from AFEM with additional MD results from literature.

4.2 Mechanical Behaviour of GNRs

In this section, the mechanical behavior of GNRs of different dimensions is examined to study the effects of size and chirality on the elastic modulus and tensile strength. The results are based on the AFEM using the second generation REBO potential. The geometry of a typical GNR is shown in Fig. 1 where l and b denotes the length and width; and N_l and N_b denote the number of hexagonal cells in the length and width directions respectively. In the numerical study, N_l = 16 with N_b equal to 3, 5, 7, 9, 11 and 17 re used to study the size effects of GNRs. Figure 8 shows the stress-strain curves of armchair and zigzag GNRs with varying values of N_b. Figure 9 shows the variation of tensile strength and elastic modulus with N_b. It is found that armchair GNRs shows little size-dependency of design properties whereas the size dependency is more prominent in the case of zigzag GNRs. This behavior agrees with the MD results reported by Zhao et al. (2009) for square GNRs and Chu et al. (2014) for both square and rectangular GNRs. Zigzag GNRs becomes stiffer as the width is reduced and the tensile strength is

also increased as shown in Fig. 9. Zigzag GNRs have a higher tensile strength compared to armchair similar to the case of bulk graphene.

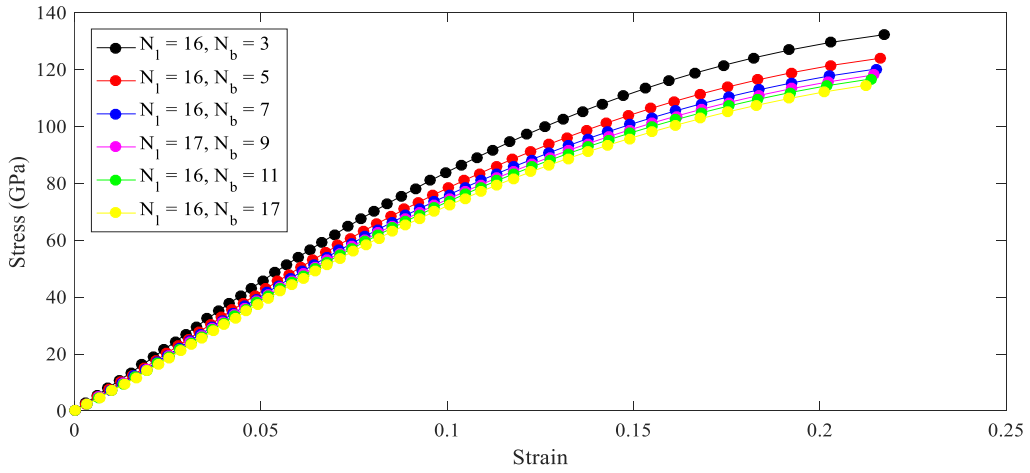

(a) Zigzag direction

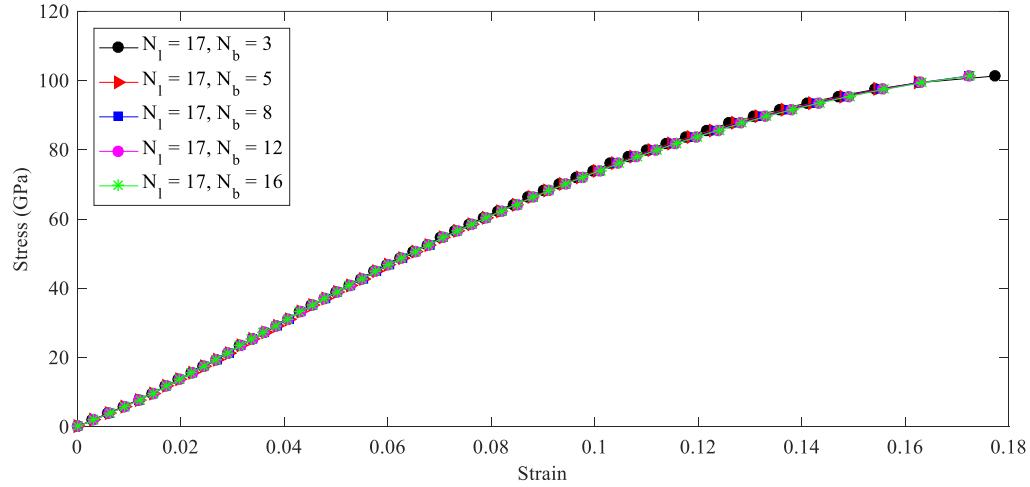

(b) Armchair direction

Figure 8: Stress-strain curves of armchair and zigzag GNRs

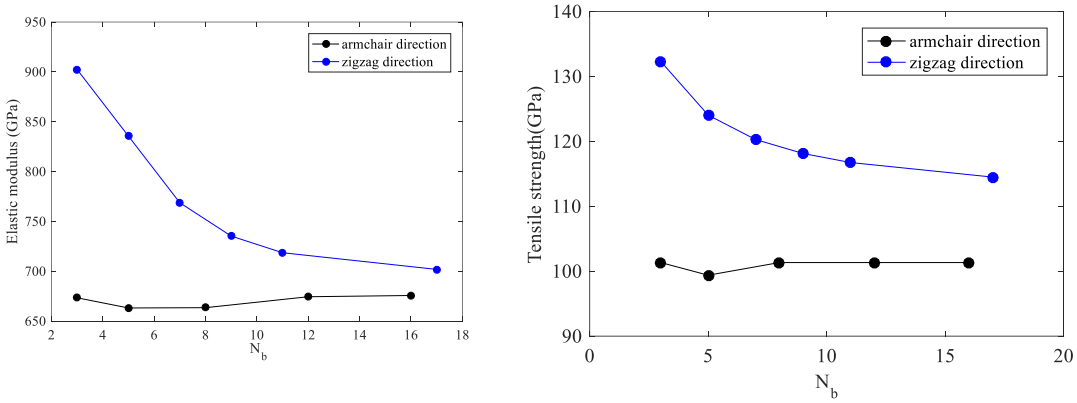

Figure 9. Variation of elastic modulus and tensile strength of GNRs with different widths.

However, it is interesting to note that the size dependency trend seen in Fig. 9 for tensile strength and elastic modulus of zigzag GNRs is different from the trend observed by Zhao et al. (2009) and Chu

et al. (2014) who reported increases in tensile strength and elastic modulus as the size of GNR increases eventually approaching the bulk values. Although Zhao et al. (2009) used square GNRs in their simulation, Chu et al. (2014) used both square and rectangular GNRs to confirm their results. In order to investigate this difference, we present a comparison of MD results based on the second generation REBO potential with our AFEM results for GNRs in Fig. 10. The accuracy of AFEM solutions is again clear from Fig. 10. The trend we notice in Fig. 9 is similar to the experimental results of Shin et al. (2006) who determined the elastic modulus of single nanofibers with an ellipsoidal cross-section using an atomic force microscope. Their results confirm a substantial increase in the elastic modulus as the dimeter of the fiber decreased similar to the trend noted in Fig. 9. It is generally reported in the literature as the size decreases the properties improve in the case of nanomaterials. Such behaviour is accounted for by an increase in the number of boundary atoms with higher energies compared to the number of internal atoms.

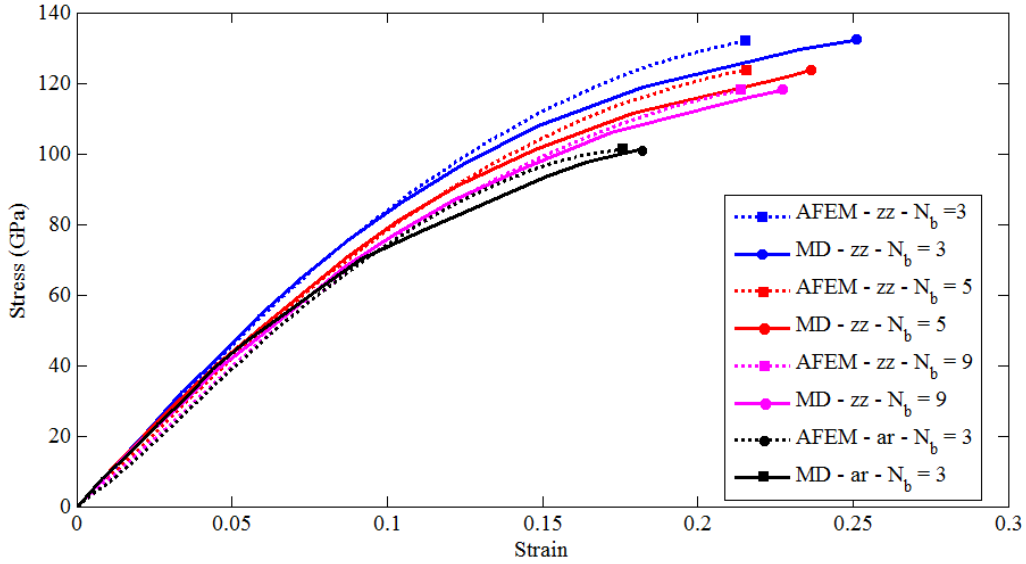

Figure 10. Comparison of GNR stress-strain curves obtined from AFEM with MD results.

Conclusions

The atomic-scale finite element method was successfully applied to study the mechanical response of GNRs. Extensive comparisons with MD simulations reported in the literature are presented for bulk graphene stress-strain curves. It is found that both AFEM and MD based on Tersoff potential are not capable of modelling the tensile behavior of graphene. The AFEM based on the second generation REBO potential shows high accuracy in modelling the tensile response of bulk graphene. Comparisons with MD solutions reported in the literature show that the tensile strength predicted by AFEM is about 5-10 % higher than the results corresponding to MD. Failure strains predicted by AFEM are generally higher than the MD results. The difference between AFEM and corresponding MD results become more visible closer to tensile failure point and hardly any difference is noted in the initial small

strain range. Armchair GNRs show negligible size-dependency whereas size-effects are significant in the case of zigzag GNRs. In terms of the chirality effects, zigzag GNRs are stiffer and stronger than armchair GNRs and similar behavior is also noted for bulk graphene. The current approach is computationally highly efficient compared to MD simulations due the O(N) characteristics of AFEM.

Acknowledgments

The study was funded by the São Paulo Research Foundation (Fapesp) through grants 2012/17948-4, 2013/23085-1, 2015/00209-2 and 2013/08293-7 (CEPID). Support from CAPES and CNPQ is also acknowledged.

References

Alzebdeh, K.: Evaluation of the in-plane effective elastic moduli of single-layered graphene sheet. Int. J. Mech. Mater. Des. 8: 269. https://doi.org/10.1007/s10999-012-9193-7 (2012).

Brenner, D.W.: Empirical potential for hydrocarbons for use in simulating the chemical vapor-deposition of diamond films. Physical Review B. 42, 9458-9471 (1990).

Brenner D.W., Shenderova O.A., Harrison, J.A., Stuart S.J., Sinnott S.B.: A second-generation reactive empirical bond order (REBO) potential energy expression for hydrocarbons. Journal of Physics: Condensed Matter. 14, 783-802 (2002).

Chen, C., Hone, J.: Graphene Nanoelectromechanical Systems. Proceedings of the IEEE, 101(7), (2013).

Choi, W., Lee, J-W. (eds.): Graphene: Synthesis and Applications, CRC Press, (2016).

Chu, Y., Ragab, T., Basaran, C.: The size effect in mechanical properties of finite-sized graphene nanoribbon. Computational Materials Science. 81, 269-274 (2014).

Dewapriya, M.A.N.: Molecular dynamics study of effects of geometric defects on the mechanical properties of graphene. Master's thesis, University of British Columbia, (2012).

Dewapriya, M.A.N., Rajapakse, R.K.N.D.: Molecular dynamics simulations and continuum modeling of temperature and strain rate dependent fracture strength of graphene with vacancy defects (2014). Int. J. Fracture. doi: 10.1115/1.4027681 (2014).

Gajbhiye, S.O., Singh, S.P.: Multiscale nonlinear frequency response analysis of single-layered graphene sheet under impulse and harmonic excitation using the atomistic finite element method. Journal of physics D: Applied physics. 48, 145305 (2015).

Gao, G.: Atomistic Studies of Mechanical Properties of Graphene. Polymers, doi:10.3390/polym6092404 (2014).

Haile, J.M.: Molecular Dynamics Simulation, Wiley, New York (1992).

Hohenberg, P., Kohn, W.: Inhomogeneous electron gas. Physical Review, 136, B864–B871 (1964).

Konstantinova, E., Dantas, S.O., Barone, P.M.V.B.: Electronic and elastic properties of two-dimensional carbon planes. Physical Review B. doi: 10.1103/PhysRevB.74.035417 (2006).

Le, M.Q.: Prediction of Young's modulus of hexagonal monolayer sheets based on molecular mechanics. Int. J. Mech. Mater. Des. 11: 15. https://doi.org/10.1007/s10999-014-9271-0 (2015).

Lee C., Wei, X., Kysar, J.W., Hone, J.: Measurement of the Elastic Properties and Intrinsic Strength of Monolayer Graphene. Science. 321, 385-388 (2008).

Liera, G.V., Alsenoyb, C.V., Dorenc V.V., Geerlingsd P.: Ab initio study of the elastic properties of single-walled carbon nanotubes and graphene. Chemical Physics Letters. 326, 181-185 (2000).

Liu, B., Huang, Y., Jiang, H., Qu, S., Hwang, K.C.: The atomic-scale finite element method. Computer Methods in Applied Mechanics and Engineering. 193, 1849-1864 (2004).

Liu, B., Jiang, H., Huang, Y., Qu, S., Yu, M.-F., Hwang, K.C.: Atomic-scale finite element method in multiscale computation with applications to carbon nanotubes. Physical Review B. 72, 035435 (2005).

Liu, F. Ming, P. Li, J.: Ab initio calculation of ideal strength and phonon instability of graphene under tension. Physical Review B. doi:10.1103/PhysRevB.76.064120 (2007).

Malakouti, M., Montazeri, A.: Nanomechanics analysis of perfect and defected graphene sheets via a novel atomic scale finite element method. Superlattices. doi: 10.1016/j.spmi.2016.03.049 (2016).

Ng, T.Y., Yeo, J. & Liu, Z.: Molecular dynamics simulation of the thermal conductivity of shorts strips of graphene and silicene: a comparative study. Int. J. Mech. Mater. Des. 9: 105. https://doi.org/10.1007/s10999-013-9215-0 (2013).

Njuguna, B., Pielichowski, K.: Polymer nanocomposites for aerospace applications: properties. Advanced Engineering Materials. 5, 769-778 (2003).

Novoselov, K.S., Geim, A.K., Morozov, S.V., Jiang, D., Zhang, Y., Dubonos, S.V., Grigorieva, I.V., Firsov, A.A.: Electric field effect in atomically thin carbon films. Science. 306, 666-669 (2004).

Shi, M.X., Li, Q.M., Liu, B., Feng, X.Q., Huang, Y.: Atomic-scale finite element analysis of vibration mode transformation in carbon nanorings and single-walled carbon nanotubes. Int. J. Solids and Structures. 46, 4342-4360 (2009)

Shin, M.K., Kim, S.I., Kim, S.J., Kim, S-K., Lee, H., Spinks, G.M.: Size-dependent elastic modulus of single electroactive polymer nanofibers. Applied Physics Letters. 89, 231929 (2006).

Stuart, S.J., Tutein, A.B., Harrison, J.A.: A reactive potential for hydrocarbons with intermolecular interactions. The Journal of Chemical Physics. 112, 6472 (2000).

Terdalkar, S.S., Shan, Huang, S., Yuan, H., Rencis, J.J., Zhu, T., Zhang, S.: Nanoscale fracture in graphene. Chemical Physics Letters. 494, 218–222 (2010).

Tersoff, J.: New empirical approach for the structure and energy of covalent systems, Physical Review B 37: 6991 (1987).

Tersoff, J.: Empirical interatomic potential for carbon with applications to amorphous carbon. Physical Review Letters. 61, 2879 (1988).

Tserpes, K.I., Papanikos, P.: Finite element modeling of single-walled carbon nanotubes. Composites Part B: Engineering. 36, 468-477 (2005).

Zhao, H., Min, K., Aluru, N.R.: Size and chirality dependent elastic properties of graphene nanoribbons under uniaxial tension. Nano Letters. 9, 3012–3015 (2009).

Appendix

Tersoff Potential Parameters:

$$f_c^T(r_{ij}) = \begin{cases} 1, & r_{ij} < R - D \\ \frac{1}{2} - \frac{1}{2}\sin\left[\frac{\pi}{2}\frac{(r_{ij} - R)}{D}\right], & R - D < r_{ij} < R + D \\ 0, & r_{ij} > R + D \end{cases} \quad \text{(A.1)}$$

The parameters *R* and *D* are not systematically optimized but are chosen so as to include the first-neighbor shell only. For C-C bonds, Tersoff (1988) presented a set of suitable values of *R* and *D* that are given below. As the parameters *R* and *D* are chosen to include only the first-neighbor interaction, thus, the cut-off function, f_c^T , goes from 1 to 0 within a cut-off distance $R\text{-}D < r_{ij} < R\text{+}D$.

$$\zeta_{ij}^{n_T} = \sum_{k \neq i,j} f_c(r_{ik})\, g(\theta_{ijk}); \; g(\theta_{ijk}) = 1 + \frac{c^2}{d^2} - \frac{c^2}{\left[d^2 + (h - \cos\theta_{ijk})^2\right]} \quad \text{(A.2)}$$

The bond angle θ_{ijk} is defined as shown in Fig. A1.

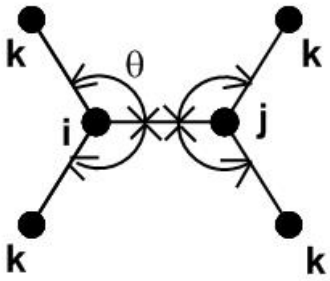

Figure A1: Definition of angles in Tersoff potential.

For carbon-carbon interactions these parameters are *A=1393.6 eV, B=346.74 eV,* λ^1*=3.4879,* λ^2*=2.2119, R=1.95 Å, D= 0.15 Å,* β^{n_T} *=1.5724 x* 10^{-7}*,* n_t *=0.72751,* c*=3.8049 x* 10^4*, d=4.3484* and *h=-0.57058* (Tersoff 1988).

Second Generation REBO Potential Parameters:

$$f_c^R\left(r_{ij}\right)=\begin{cases}1, & r_{ij}<R^{(1)}\\ \dfrac{\left[1+\cos\left[\dfrac{\pi\left(r_{ij}-R^{(1)}\right)}{\left(R^{(2)}-R^{(1)}\right)}\right]\right]}{2} & R^{(1)}<r_{ij}<R^{(2)}\\ 0, & R^{(2)}<r_{ij}\end{cases} \tag{A.3}$$

The term B^R corresponds to the bond order term. It's related with the number of neighbors and the angle, which it's related with the forming and breaking of the bonds between of the atoms. The expression for B^R is:

$$B^R=\frac{1}{2}\left[b_{ij}^{\sigma\pi}+b_{ji}^{\sigma\pi}\right]+b_{ij}^{\pi} \tag{A.4}$$

$$b_{ij}^{\pi}=\Pi_{ij}^{rc}+b_{ij}^{dh} \tag{A.5}$$

The term $b_{ij}^{\sigma\pi}$ is composed by covalent bond interactions, and by the angular function $g\left(cos\theta_{jik}\right)$, which include the contribution from the second nearest neighbour according to the cosine of the angle of the bonds between atoms *ik* and *ij*.

$$b_{ij}^{\sigma\pi}=\left[1+\sum_{k\neq i,j}f_{ik}\left(r_{ik}\right)g\left(cos\theta_{jik}\right)e^{\lambda_{ijk}}+P_{ij}\left(N_i^C,N_i^H\right)\right]^{-\frac{1}{2}} \tag{A.6}$$

According to Brenner et al. (2002) the parameters P_{ij} and λ_{ijk} are taken to be zero for solid-state carbon. The following equations show the angular function in three regions of bond angle θ,

For $0^o<\theta<109.476^o$

$$g\left(cos\theta_{jik}\right)=G\left(cos\theta_{jik}\right)+Q\left(N_i^t\right)\left[\gamma\left(cos\theta_{jik}\right)-G\left(cos\theta_{jik}\right)\right] \tag{A.7}$$

$$G\left(cos\theta_{jik}\right)=0.5024cos^5\left(\theta\right)+1.4297cos^4\left(\theta\right)+2.0313cos^3\left(\theta\right)+2.2544cos^2\left(\theta\right)+1.4068cos\left(\theta\right)+0.3755 \tag{A.8}$$

$$\gamma\left(cos\theta_{jik}\right)=-0.0401cos^5\left(\theta\right)+1.272cos^4\left(\theta\right)-0.5597cos^3\left(\theta\right)-0.4331cos^2\left(\theta\right)+0.4889cos\left(\theta\right)+0.2719 \tag{A.9}$$

For $109.476^o < \theta < 120^o$

$$g\left(cos\theta_{jik}\right) = G\left(cos\theta_{jik}\right)$$

$$G\left(cos\theta_{jik}\right) = 36.2789cos^5\left(\theta\right) + 71.8829cos^4\left(\theta\right) + 57.5918cos^3\left(\theta\right) + 24.0970cos^2\left(\theta\right) + 5.6774cos\left(\theta\right) + 0.7073 \tag{A.10}$$

For $120^o < \theta < 180^o$

$$g\left(cos\theta_{jik}\right) = G\left(cos\theta_{jik}\right) \tag{A.11}$$

$$G\left(cos\theta_{jik}\right) = -1.3424cos^5\left(\theta\right) - 4.928cos^4\left(\theta\right) - 6.83cos^3\left(\theta\right) - 4.346cos^2\left(\theta\right) - 1.098cos\left(\theta\right) + 0.0026 \tag{A.12}$$

The function $Q\left(N_i^t\right)$ is given by

$$Q\left(N_i^t\right) = \begin{cases} 1 & N_i^t < 3.2 \\ \left[1 + cos\left(2\pi\left(N_i^t - 3.2\right)\right)\right]/2 & 3.2 < N_i^t < 3.7 \\ 0 & N_i^t > 3.7 \end{cases} \tag{A.13}$$

The term N_i^t is the sum of the carbon atoms number and the hydrogen atoms number, in this case N_i^H is zero,

$$N_i^t = N_i^C + N_i^H \tag{A.14}$$

$$N_i^C = \sum_{k(\neq i,j)}^{carbon\ atoms} f_{ik}\left(r_{ik}\right) \tag{A.15}$$

The term Π_{ij}^{rc} is a three-dimensional cubic spline, which depends on the number of carbon atoms that are neighbors of atoms *i* and *j* and the nonconjugated bonds.

$$\Pi_{ij}^{rc} = F_{ij}\left(N_i^t, N_j^t, N_{ij}^{conj}\right) \tag{A.16}$$

$$N_{ij}^{conj} = 1 + \left[\sum_{k(\neq i,j)}^{carbon\ atoms} f_{ik}\left(r_{ik}\right) F\left(x_{ik}\right) \right]^2 + \left[\sum_{l(\neq i,j)}^{carbon\ atoms} f_{jl}\left(r_{jl}\right) F\left(x_{jl}\right) \right]^2 \tag{A.17}$$

$$F\left(x_{ik}\right) = \begin{cases} 1 & x_{ik} < 2 \\ \left[1 + \cos\left(2\pi\left(x_{ik} - 2\right)\right)\right] / 2 & 2 < x_{ik} < 3 \\ 0 & x_{ik} > 3 \end{cases} \tag{A.18}$$

$$x_{ik} = N_k^t - f_{ik}\left(r_{ik}\right) \tag{A.19}$$

where *k*, *l*, and *j* are the neighbors of atoms.

The term b_{ij}^{dh} is zero for graphene due to its planar configuration. All the parameters considered can be found in Stuart et al. (2000).